

High-speed modulation in ladder transitions in Rb atoms using high-pressure buffer gas

Subramanian Krishnamurthy,¹ Y. Wang,¹ Y. Tu,¹ S. Tseng,¹ and M. S. Shahriar^{1,2,*}

¹Department of EECS, Northwestern University, Evanston, Illinois 60208, USA

²Department of Physics and Astronomy, Northwestern University, Evanston, Illinois 60208, USA
*shahriar@northwestern.edu

Abstract: Modulators using atomic systems are often limited in speed by the rate of spontaneous emission. One approach for overcoming this limit is to make use of a buffer gas such as Ethane, which causes rapid fine structure mixing of the $P_{1/2}$ and $P_{3/2}$ states, and broadens the absorption spectra of the D1 and D2 lines in alkali atoms. Employing this effect, we show that one can achieve high speed modulation using ladder transitions in Rubidium. We demonstrate a 100-fold increase, due to the addition of the buffer gas, in the modulation bandwidth using the 5S-5P-5D cascade system. The observed bandwidth of ~ 200 MHz is within a factor of 2.5 of the upper bound of ~ 0.51 GHz for the system used, and is limited by various practical constraints in our experiment. We also present numerical simulations for the system and predict that a much higher modulation speed should be achievable under suitable conditions. In combination with a tapered nano fiber or a SiN waveguide, it has the potential to be used for high-speed, low-power all-optical modulation.

© 2015 Optical Society of America

OCIS codes: (020.4180) Multiphoton processes; (250.4110) Modulators.

References and links

1. S. E. Harris and Y. Yamamoto, "Photon switching by quantum interference," *Phys. Rev. Lett.* **81**(17), 3611–3614 (1998).
2. R. G. Beausoleil, W. J. Munro, D. A. Rodrigues, and T. P. Spiller, "Applications of electromagnetically induced transparency to quantum information processing," *J. Mod. Opt.* **51**(16-18), 2441–2448 (2004).
3. A. M. C. Dawes, L. Illing, S. M. Clark, and D. J. Gauthier, "All-optical switching in rubidium vapor," *Science* **308**(5722), 672–674 (2005).
4. M. Bajcsy, S. Hofferberth, V. Balic, T. Peyronel, M. Hafezi, A. S. Zibrov, V. Vuletic, and M. D. Lukin, "Efficient all-optical switching using slow light within a hollow fiber," *Phys. Rev. Lett.* **102**(20), 203902 (2009).
5. V. Venkataraman, P. Londero, A. R. Bhagwat, A. D. Slepikov, and A. L. Gaeta, "All-optical modulation of four-wave mixing in an Rb-filled photonic bandgap fiber," *Opt. Lett.* **35**(13), 2287–2289 (2010).
6. S. Krishnamurthy, Y. Wang, Y. Tu, S. Tseng, and M. S. Shahriar, "High efficiency optical modulation at a telecom wavelength using the quantum Zeno effect in a ladder transition in Rb atoms," *Opt. Express* **20**(13), 13798–13809 (2012).
7. S. Krishnamurthy, Y. Wang, Y. Tu, S. Tseng, and M. S. Shahriar, "Optically controlled polarizer using a ladder transition for high speed Stokesmetric Imaging and Quantum Zeno Effect based optical logic," *Opt. Express* **21**(21), 24514–24531 (2013).
8. S. Krishnamurthy, Y. Tu, Y. Wang, S. Tseng, and M. S. Shahriar, "Optically controlled waveplate at a telecom wavelength using a ladder transition in Rb atoms for all-optical switching and high speed Stokesmetric imaging," *Opt. Express* **22**(23), 28898–28913 (2014).
9. K. Salit, M. Salit, S. Krishnamurthy, Y. Wang, P. Kumar, and M. S. Shahriar, "Ultra-low power, Zeno effect based optical modulation in a degenerate V-system with a tapered nano fiber in atomic vapor," *Opt. Express* **19**(23), 22874–22881 (2011).
10. S. M. Spillane, G. S. Pati, K. Salit, M. Hall, P. Kumar, R. G. Beausoleil, and M. S. Shahriar, "Observation of nonlinear optical interactions of ultralow levels of light in a tapered optical nanofiber embedded in a hot rubidium vapor," *Phys. Rev. Lett.* **100**(23), 233602 (2008).
11. G. Brambilla, V. Finazzi, and D. Richardson, "Ultra-low-loss optical fiber nanotapers," *Opt. Express* **12**(10), 2258–2263 (2004).
12. S. M. Hendrickson, M. M. Lai, T. B. Pittman, and J. D. Franson, "Observation of two-photon absorption at low power levels using tapered optical fibers in rubidium vapor," *Phys. Rev. Lett.* **105**(17), 173602 (2010).

13. B. V. Zhdanov and R. J. Knize, "Progress in alkali lasers development," Proc. SPIE **6874**, 68740F(2008).
14. R. J. Beach, W. F. Krupke, V. K. Kanz, S. A. Payne, M. A. Dubinskii, and L. D. Merkle, "End-pumped continuous-wave alkali vapor lasers: experiment, model, and power scaling," J. Opt. Soc. Am. B **21**(12), 2151–2163 (2004).
15. E. Walentynowicz, R. A. Phaneuf, and L. Krause, "Inelastic collisions between excited alkali atoms and molecules. X. Temperature dependence of cross sections for $2P_{3/2}$ - $2P_{1/2}$ mixing in cesium, induced in collisions with deuterated hydrogens, Ethanes, and propanes," Can. J. Phys. **52**, 589–591 (1974).
16. S.-Y. Chen and M. Takeo, "Broadening and shift of spectral lines due to the presence of foreign gases," Rev. Mod. Phys. **29**(1), 20–73 (1957).
17. M. V. Romalis, E. Miron, and G. D. Cates, "Pressure broadening of Rb D1 and D2 lines by ^3He , ^4He , N_2 , and Xe: line cores and near wings," Phys. Rev. A **56**(6), 4569–4578 (1997).
18. M. S. Shahriar, Y. Wang, Y. Subramanian Krishnamurthy, Y. Tu, G. S. Pati, and S. Tseng, "Evolution of an n-level system via automated vectorization of the Liouville equations and application to optically controlled polarization rotation," J. Mod. Opt. **61**(4), 351–367 (2014).
19. D. A. Steck, "Alkali D line data," <http://steck.us/alkalidata/rubidium87numbers.pdf>
20. P. Kulatunga, H. C. Busch, L. R. Andrews, and C. I. Sukenik, "Two-color polarization spectroscopy of rubidium," Opt. Commun. **285**(12), 2851–2853 (2012).
21. X. Hu, P. Jiang, C. Ding, H. Yang, and Q. Gong, "Picosecond and low-power all-optical switching based on an organic photonic-bandgap microcavity," Nat. Photonics **2**(3), 185–189 (2008).
22. A. M. C. Dawes, L. Illing, S. M. Clark, and D. J. Gauthier, "All-Optical Switch Controls Strong Beams with Weak Ones," OPN, p 24, (2005).
23. Q. Xu and M. Lipson, "All-optical logic based on silicon micro-ring resonators," Opt. Express **15**(3), 924–929 (2007).
24. M. Bajcsy, S. Hofferberth, V. Balic, T. Peyronel, M. Hafezi, A. S. Zibrov, V. Vuletic, and M. D. Lukin, "Efficient all-optical switching using slow light within a hollow fiber," Phys. Rev. Lett. **102**(20), 203902 (2009).
25. B. V. Zhdanov, T. Ehrenreich, and R. J. Knize, "Highly efficient optically pumped cesium vapor laser," Opt. Commun. **260**(2), 696–698 (2006).
26. J. T. Verdeyen, *Laser Electronics* (Prentice Hall, 1995)
27. W. F. Krupke, "Diode Pumped Alkali Lasers (DPALs) – an Overview," Proc. SPIE **7005**, 700521 (2008).
28. Z. Konefal, "Observation of collision induced processes in rubidium–Ethane vapour," Opt. Commun. **164**(1-3), 95–105 (1999).
29. F. Nez, F. Biraben, R. Felder, and Y. Millerioux, "Optical frequency determination of the hyperfine components of the $5S_{1/2}$ - $5D_{3/2}$ two-photon transitions in rubidium," Opt. Commun. **102**(5-6), 432–438 (1993).
30. F. Nez, F. Biraben, R. Felder, and Y. Millerioux, "Optical frequency determination of the hyperfine components of the $5S_{1/2}$ - $5D_{3/2}$ two-photon transitions in rubidium: erratum," Opt. Commun. **110**(5-6), 731 (1994).
31. H. S. Moon and H. R. Noh, "Optical pumping effects in ladder-type electromagnetically induced transparency of $5S_{1/2}$ - $5P_{3/2}$ - $5D_{3/2}$ transition of ^{87}Rb atoms," J. Phys. At. Mol. Opt. Phys. **44**(5), 055004 (2011).
32. R. Hamid, M. Cetintas, and M. Celik, "Polarization resonance on S–D two-photon transition of Rb atoms," Opt. Commun. **224**(4-6), 247–253 (2003).
33. J. E. Bjorkholm and P. F. Liao, "Line shape and strength of two-photon absorption in an atomic vapor with a resonant or nearly resonant intermediate state," Phys. Rev. A **14**(2), 751–760 (1976).
34. L. Stern, B. Desiatov, I. Goykhman, and U. Levy, "Nanoscale light-matter interactions in atomic cladding waveguides," Nat. Commun. **4**, 1548 (2013).

1. Introduction

All-optical modulation and switching are important for optical communication and quantum information processing [1–5]. We have already demonstrated a cascade system all-optical modulator, polarizer and waveplate at a telecommunication wavelength using the $5S_{1/2}$ - $5P_{1/2}$ - $6S_{1/2}$ system, where the lower leg, at 795 nm, controls the transmission and absorption of the upper leg at 1323 nm [6–8]. We verified experimentally that the bandwidth for the modulator is limited by the decay rate (~ 6 MHz) of the intermediate level [6]. We also proposed a novel scheme for increasing the modulation bandwidth using buffer gas induced rapid fine structure mixing [6]. In this paper, we present experimental results for such a modulator using the $5S_{1/2}$ - $5P_{3/2}$ - $5D_{3/2}$ system, where the lower leg is at 780 nm and the upper leg is at ~ 776 nm. The process is aided by the presence of the $5P_{1/2}$ level. The choice of these particular transitions is primarily determined by the operational wavelength of the devices at our disposal. The principle of operation is the same for any cascade system with two intermediate fine structure levels, and thus can be used at a wavelength corresponding to the telecommunication band, for example. In combination with a tapered nano fiber (TNF)

system [9–12], the system has the potential to be used for low-power high-speed all-optical switching.

The rest of the paper is organized as follows. In section 2, we briefly review the effects of buffer gas on alkali atoms. In section 3, we present a detailed model for our system and show simulation results. The details of the experimental set-up and the spectral information corresponding to the 5S-5P-5D system are presented in section 4. In section 5, we present the experimental results, including spectral data and modulation data with and without buffer gas. We discuss means to improve the system performance in section 6 and present our conclusions in section 7.

2. Effect of high-pressure buffer gas on alkali metals

It is well known that in the presence of high pressure buffer gas, there is rapid inter-mixing and dephasing of atoms in the $5P_{3/2}$ and the $5P_{1/2}$ states of alkali metals [13–17]. For concreteness, we restrict our discussion to the case where the buffer gas used is Ethane, and the alkali atom of interest is ^{85}Rb . The behavior of ^{87}Rb as well as other alkali atoms, and under the presence of different buffer gases, is qualitatively similar, while differing in details. Relevant parameters for ^{87}Rb as well as other alkali atoms can be found in [14], [26] and [27].

Consider a vapor cell loaded with ^{85}Rb and Ethane buffer gas at 300 Torr, and a temperature of about 150° C. These parameters are close to those used in the experiment. We consider first the three lowest energy manifolds: $5S_{1/2}$, $5P_{1/2}$ and $5P_{3/2}$, indicated as states $|A\rangle$, $|B\rangle$ and $|C\rangle$, respectively, as shown in Fig. 1. Since the buffer gas induced width of the absorption spectrum under such conditions will be much broader than the hyperfine splitting within each of these three manifolds, we can treat each of them as a single energy level. When excited by a pump at the D2 line (i.e., the A-C transition), the presence of the buffer gas causes the following two effects.

First, the coherence generated between states $|A\rangle$ and $|C\rangle$ dephases rapidly, without affecting the rate at which atoms in state $|A\rangle$ decay radiatively to level $|C\rangle$ via spontaneous emission. The radiative decay rate, denoted by Γ_R , is the inverse of the radiative lifetime of ~ 27 nsec, so that $\Gamma_R \approx 37 \times 10^6 \text{ sec}^{-1}$ [19,20]. The dephasing rate, denoted by Γ_D , is determined by the pressure of the buffer gas. For Ethane, this dephasing rate is about $2\pi \times 2 \times 10^7 \text{ sec}^{-1}/\text{Torr}$ (20 MHz/Torr) [25,26], so that the rate at 300 Torr is $\Gamma_D \approx 2\pi \times 6 \times 10^9 \text{ sec}^{-1}$ (6 GHz). Taking into account the fact that the Doppler width is about 0.6 GHz, and that the $5S_{1/2}$ manifold has a hyperfine splitting of about 3 GHz, this dephasing would produce an absorption profile on the A-C leg with a width of at least 9.6 GHz, in the limit of a weak pump. Of course, essentially the same effect is present on the A-B leg. The state $|B\rangle$ decays radiatively at almost the same rate ($\sim 37 \times 10^6 \text{ sec}^{-1}$) as that of state $|C\rangle$, while the A-B coherence decays at the same dephasing rate (Γ_D) as that of the A-C coherence. As such, the absorption profile on the A-B leg also has a width of about 9.6 GHz at this pressure of Ethane. It should be noted that the absorption profile on each of these legs would be widened further due to additional dephasing attributed to the radiative and collisional relaxation of populations in states $|B\rangle$ and $|C\rangle$, as discussed later.

Second, states $|B\rangle$ and $|C\rangle$ decay into each other at a rate determined by the pressure of the buffer gas. The rate of decay from $|C\rangle$ to $|B\rangle$, denoted as Γ_{CB} , is about $1.07 \times 10^7 \text{ sec}^{-1}/\text{Torr}$ [14]. Thus, for a pressure of 300 Torr, we have $\Gamma_{CB} \approx 3.21 \times 10^9 \text{ sec}^{-1}$ (~ 0.51 GHz). This is nearly a factor of 87 times faster than the rate of radiative decay from $|C\rangle$ to $|A\rangle$. The rate of decay from $|B\rangle$ to $|C\rangle$ is determined by assuming that, in the limit of vanishingly small optical excitation applied on the A-C leg, the populations of all the energy levels will correspond to a thermal equilibrium, obeying Boltzmann statistics. Given that the number of Zeeman sublevels in the $5P_{3/2}$ manifold is twice as large as the number of Zeeman sublevels in the $5P_{1/2}$ manifold, we thus get $\Gamma_{BC} / \Gamma_{CB} = 2 \times \exp(-\Delta E / k_B T)$, where ΔE is the energy difference between states $|C\rangle$ and $|B\rangle$, k_B is the Boltzmann constant, and T is the temperature

in Kelvin [14]. For ^{85}Rb , we have $\Delta E/k_B \approx 341.1$ Kelvin. Thus, at 150°C , we get that $\Gamma_{BC}/\Gamma_{CB} \approx 0.89$, so that $\Gamma_{BC} \approx 2.86 \cdot 10^9 \text{ sec}^{-1}$ (~ 0.46 GHz). Of course, the actual ratio of populations between state $|C\rangle$ and state $|B\rangle$ will differ from the thermal equilibrium value of Γ_{BC}/Γ_{CB} due to the presence of the (typically strong) pump along the A-C transition (as well as possibly other optical fields that may be present or generated).

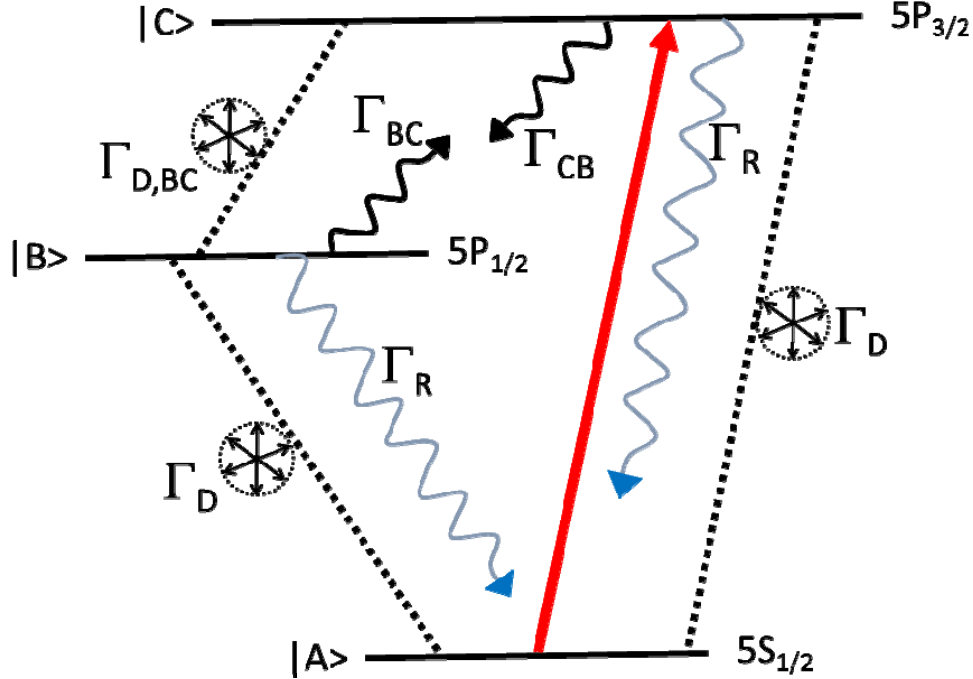


Fig. 1. Schematic illustration of the population and coherence dynamics in an alkali atom in the presence of a high-pressure buffer gas.

It should be noted that the exchange of populations between states $|B\rangle$ and $|C\rangle$ automatically implies that any coherence that could possibly be generated between states $|B\rangle$ and $|C\rangle$ (e.g., in the presence of another pump acting along the A-B leg which is phase coherent with the pump along the A-C leg) would decay as well. We denote this decay rate as $\Gamma_{D,BC}$. The minimum value of the decay rate is $\Gamma_{D,BC,MIN} = (\Gamma_{BC} + \Gamma_{CB})/2$, which in this case corresponds to a rate of $\sim 3.04 \cdot 10^9 \text{ sec}^{-1}$ [18]. In principle, the actual dephasing rate of the B-C coherence could be much larger, given the fact that the collision-induced dephasing rate Γ_D of the A-B (as well as the A-C) coherence is nearly a factor of 12.4 larger. Thus, we can write $\Gamma_{D,BC} = \Gamma_{D,BC,MIN} + \alpha\Gamma_D$, where α is a parameter the value of which depends on the details of the collision process that generates the dephasing of the A-B and A-C transition. Theoretical studies carried out so far [14,16,28] do not provide any clear indication regarding the value of α . Furthermore, to the best of our knowledge, no experimental study to determine the value of α has been carried out yet. Fortunately, for the experiment described in this paper, no coherence is generated between states $|B\rangle$ and $|C\rangle$. As such, the value of α as well as the value of $\Gamma_{D,BC}$ does not affect the experimental results, nor the outcome of the simulations thereof.

Along the same line, we denote by $\Gamma_{D,AC}$ ($\Gamma_{D,AB}$) the net rate at which the A-C (A-B) coherence would dephase. Accounting for the additional dephasing caused by the decay of populations from state $|C\rangle$, we thus get that $\Gamma_{D,AC} = \Gamma_D + (\Gamma_R + \Gamma_{CB})/2$. Similarly, we get that $\Gamma_{D,AB} = \Gamma_D + (\Gamma_R + \Gamma_{BC})/2$. Since the value of Γ_R is much smaller than the other rates, we see

that $\Gamma_{D,AC} \approx \Gamma_D + \Gamma_{CB}/2$ and $\Gamma_{D,AB} \approx \Gamma_D + \Gamma_{BC}/2$. Thus, the spectrum profile on the A-C (A-B) leg will be broadened further by $\Gamma_{CB}/2$ ($\Gamma_{BC}/2$), in addition to the 9.6 GHz estimated above.

Finally, we note that all the decay and dephasing timescales for ^{87}Rb are very similar to those described above for ^{85}Rb . Thus, even though the experiment described here makes use of a natural mixture of both of these isotopes (72.16% of ^{85}Rb and 27.84% of ^{87}Rb), we treat our system, in simulations, as if it is made entirely of ^{85}Rb .

3. Modeling and simulation results

For realizing a high-speed optical modulator, we make use of the system described above, augmented by another transition coupling the $5P_{3/2}$ state to the $5D_{3/2}$ state. The control beam is applied on the $5S_{1/2}$ - $5P_{3/2}$ leg, and the signal beam is applied on the $5P_{3/2}$ - $5D_{3/2}$ leg. This system is illustrated schematically in Fig. 2. On the left, we show only the population decay rates. On the right, we show additional dephasing of the coherences among the various states, without corresponding decays of the populations of these states. The exact meaning of these various dephasing rates can be deciphered from the density matrix equations for these states and is described later.

As shown in Fig. 2(a), the population of state $|2\rangle$ decays to level $|1\rangle$ radiatively at the rate of γ_a , which is the same as Γ_R shown in Fig. 1. In addition, it decays to state $|4\rangle$, via collision with Ethane atoms, at the rate of γ_{down} , which is the same as Γ_{CB} shown in Fig. 1. Similarly, population of state $|4\rangle$ decays radiatively to state $|1\rangle$ at the rate of γ_a ($= \Gamma_R$), and to state $|2\rangle$ collisionally at the rate of γ_{up} ($= \Gamma_{BC}$). Finally, state $|3\rangle$ decays radiatively to each of states $|2\rangle$ and $|4\rangle$. For simplicity, we have ignored the small difference in the branching ratios of these, and assumed that these two decay rates are the same, indicated as $\gamma_b/2$, where $\gamma_b \approx 2\pi \times 10^6 \text{ sec}^{-1}$ (1 MHz). The decay of these populations also causes corresponding decays of the coherences among these states. Specifically, if the population of state $|i\rangle$ has a net decay rate of γ_i , then the decay rate of the coherence between states $|i\rangle$ and $|j\rangle$ is given by $(\gamma_i + \gamma_j)/2$ [18].

Figure 2(b) shows the rates of additional decays for the coherences among these states, caused by collisions with Ethane atoms. For the 1-2 coherence, this rate, indicated as γ_d , is the same as Γ_D shown in Fig. 1. Similarly, for the 1-4 coherence, this rate is also γ_d ($= \Gamma_D$). For the 2-4 coherence, the rate is $\alpha\gamma_d$ ($= \alpha\Gamma_D$), where the precise value of the parameter α is not known, as discussed earlier while describing the model presented in Fig. 1. Consider next the coherences involving state $|3\rangle$, the uppermost state. We denote by $\beta\gamma_d$ ($= \beta\Gamma_D$) the dephasing rate for the 2-3 as well as the 4-3 coherence, and by $\xi\gamma_d$ ($= \xi\Gamma_D$) the dephasing rate of the 1-3 coherence, since these dephasing rates are expected to be closely related to that of the 1-2 coherence. This is because these dephasing rates are not due to population excitation or relaxation, but rather due to phase changing collisions, which should affect all coherences in a similar fashion. To the best of our knowledge, no experimental study has been carried out, nor any explicit theoretical model developed, to establish the values of the parameters β and ξ . In principle, the value of β can be established by determining the absorption profile of the 2-3 transition, as described in more detail later. However, since the 2-3 absorption can only be seen when a pump is also present on the 1-2 transition, any inference regarding the 2-3 dephasing rate would depend on the parameters of the 1-2 pump, including its power, spectrum, temporal profile, as well as correlation between its frequency and the frequency of the 2-3 probe. Thus, a systematic and extensive experimental study, aided by a theoretical model, has to be carried out to determine accurately the values of α , β and ξ . We will carry out, and report the findings of such a study in the near future.

For the purpose of the experiment and the simulation thereof reported here, we instead rely on a physical argument to estimate the values of these parameters. The dephasing of the 1-2 and 1-4 coherences are caused by collisions (between a ^{85}Rb atom and an Ethane molecule) that changes the optical transition frequencies in a random fashion. Since this can happen when the ^{85}Rb atom is any of the states, a plausible value of each of these parameters

(α , β and ξ) is unity. We have used these values in the simulations, which show that the behavior of the optical modulation is completely insensitive to the value of α (since the 2-4 coherence is always zero, as explained earlier), and relatively robust against variations in β and ξ away from the unity values.

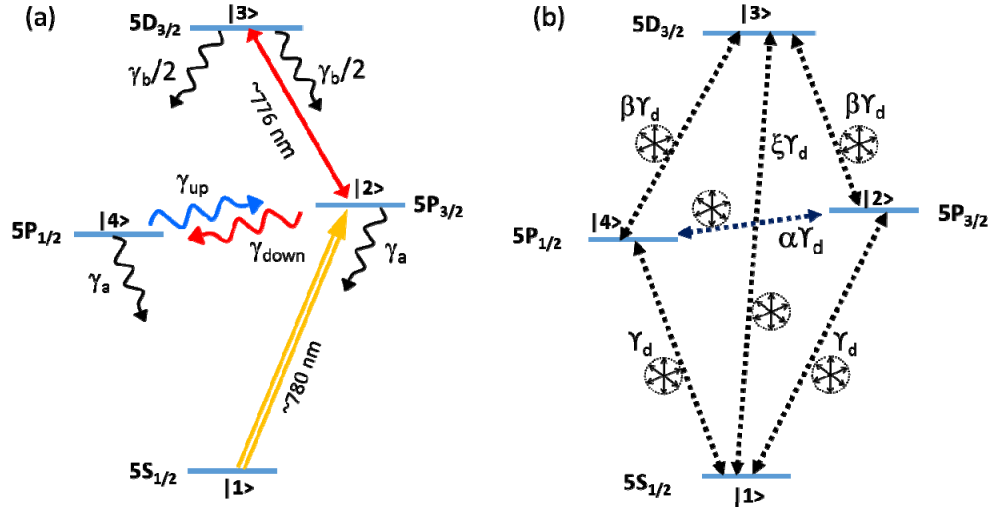


Fig. 2. Model used for numerical simulation (a) Optical fields and decay rates-radiative and collisional. (b) Transverse decay (dephasing) terms.

For our numerical simulations, we used the Liouville equation, which describes the evolution of the density matrix, given the Hamiltonian. We follow the prescription described in [18] and accordingly, the density matrix evolution is represented by

$$\frac{\partial}{\partial t} \tilde{\rho} = \frac{\partial}{\partial t} \tilde{\rho}_{ham} + \frac{\partial}{\partial t} \tilde{\rho}_{source} + \frac{\partial}{\partial t} \tilde{\rho}_{trans-decay} \quad (1)$$

where

$$\frac{\partial}{\partial t} \tilde{\rho}_{ham} = -\frac{i}{\hbar} [H' \tilde{\rho} - \tilde{\rho} H'^*] \quad (2)$$

and H' is the Hamiltonian under the Rotating Wave Approximation and in a basis which is rotating at the optical frequency. In our case, it is given by

$$H' = \begin{pmatrix} 0 & \Omega_a / 2 & 0 & 0 \\ \Omega_a / 2 & -i\gamma_2 / 2 & \Omega_b / 2 & 0 \\ 0 & \Omega_b / 2 & -i\gamma_3 / 2 & 0 \\ 0 & 0 & 0 & -i\gamma_4 / 2 \end{pmatrix} \quad (3)$$

Here, γ_2 is the sum of the radiative decay and buffer gas induced collisional decay i.e. $\gamma_2 = \gamma_a + \gamma_{down}$. Similarly, $\gamma_4 = \gamma_a + \gamma_{up}$. The addition of the decay terms to the diagonal elements of the Hamiltonian is a convenient way of taking into account the decay of atomic populations, and the corresponding decay of the relevant coherences [18]. Finally, following the convention in [18], the source terms and transverse decay terms in Eq. (1) can be represented in matrix forms by Eqs. (4) and (5) respectively:

$$\frac{\partial}{\partial t} \tilde{\rho}_{source} = \begin{pmatrix} \gamma_a (\tilde{\rho}_{22} + \tilde{\rho}_{44}) & 0 & 0 & 0 \\ 0 & (\gamma_b \tilde{\rho}_{33} / 2 + \gamma_{up} \tilde{\rho}_{44}) & 0 & 0 \\ 0 & 0 & 0 & 0 \\ 0 & 0 & 0 & (\gamma_b \tilde{\rho}_{33} / 2 + \gamma_{down} \tilde{\rho}_{22}) \end{pmatrix} \quad (4)$$

$$\frac{\partial}{\partial t} \tilde{\rho}_{trans-decay} = \begin{pmatrix} 0 & -\gamma_d \tilde{\rho}_{12} & -\xi \gamma_d \tilde{\rho}_{13} & -\gamma_d \tilde{\rho}_{14} \\ -\gamma_d \tilde{\rho}_{21} & 0 & -\beta \gamma_d \tilde{\rho}_{23} & -\alpha \gamma_d \tilde{\rho}_{24} \\ -\xi \gamma_d \tilde{\rho}_{31} & -\beta \gamma_d \tilde{\rho}_{32} & 0 & -\beta \gamma_d \tilde{\rho}_{34} \\ -\gamma_d \tilde{\rho}_{41} & -\alpha \gamma_d \tilde{\rho}_{42} & -\beta \gamma_d \tilde{\rho}_{43} & 0 \end{pmatrix} \quad (5)$$

A typical result of the simulation using this model is presented in Fig. 3, for a square modulation at 1 GHz. The red trace represents the pump while the blue trace is the probe. Here, we have used the values of the relevant parameters for temperature of 150° C, and an Ethane pressure of 300 Torr, and have used $\alpha = \beta = \xi = 1$. The pump Rabi frequency was chosen to be $\Omega_p = 8000\gamma_a$. The probe Rabi frequency was chosen to be $0.1\gamma_a$. While we have indicated the vertical axis as having arbitrary units, it should be noted that the Rabi frequencies, which correspond to the square root of the intensities, are specified above. Since this is an absorptive modulation, the degree of absorption can be increased by increasing the optical density, via using either a longer cell length or a larger density. The modulation depth, which is about 90% as shown, can easily be made to be essentially 100%, as is the case for virtually any absorptive modulator.

Such a modulator can exhibit a wide range of behavior, depending on the choice of parameters. In [6], where we first proposed the concept of realizing a high-speed modulator using a ladder transition and a buffer gas, we discussed in great detail, in section 6, the range of behavior that can be expected, and the physical explanations thereof. We also considered, in [6], the case where a re-shelving pump is employed to depopulate level $|4\rangle$ rapidly, following the turning off of the pump, and showed that the modulation works with or without the re-shelving pulses, albeit with differing modulation depths for a given optical density (in this context, it should again be noted that for an absorptive modulator, any desired modulation depth can be achieved by increasing the optical density). It should also be noted that in [6], we considered a model system, while, in this paper, we are considering a specific system. In what follows, we summarize the most salient features of the behavior of this modulator.

First, the modulation bandwidth is determined primarily by the decay rate of $|2\rangle$ to state $|4\rangle$, which is indicated as γ_{down} in Fig. 2. In the case considered here, this rate is 0.51 GHz. Second, the collisional dephasing rate of the 1-2 coherence (which, in this case, is $\gamma_d = 9.6$ GHz), does not determine, nor affect significantly, the bandwidth of the modulation. However, a large value of this rate allows more efficient absorption of a high bandwidth pump pulse. Third, for most efficient modulation for a given optical density, the pump Rabi frequency should be close to γ_d . However, this is not a fundamental constraint. Since this is an absorptive modulator, any degree of modulation amplitude at a given optical density can be increased to a modulation depth of near 100% by increasing the optical density. This can be achieved by increasing the temperature of the cell, or by increasing the interaction length. Fourth, the transient response (i.e., the ringing) of the probe is affected by two parameters. As explained in detail in [6], the ringing that occurs after the pump is turned on, happens at the rate of the pump Rabi frequency. For the pump Rabi frequency used here ($\Omega_p = 8000\gamma_a$), this corresponds to a time scale of about 0.02 nanoseconds, which is roughly the time scale of these oscillation seen in Fig. 3. On the other hand, the ringing that is seen to occur after the pump is turned off is due to the fact that we have used rectangular profiles for the pump pulses, which has spectral components that exceed the bandwidth of the homogeneous absorption (~ 9.6 GHz) along the 1-2 transition. In a real experiment, the applied pulses would

be smooth, and these ringing would be suppressed strongly if the rise and fall times of the applied pulses are slower than the inverse of this bandwidth.

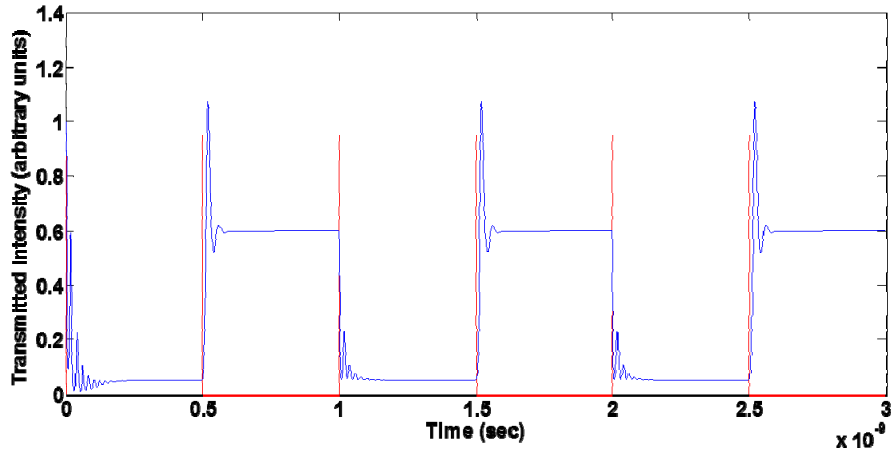


Fig. 3. Simulation results for high speed modulator at 1 GHz. Red trace: pump; Blue trace: Probe. While we have indicated the vertical axis as having arbitrary units, it should be noted that the Rabi frequencies, which correspond to the square root of the intensities, are specified (pump Rabi frequency is $800\gamma_a$, and probe Rabi frequency is $0.1\gamma_a$). Since this is an absorptive modulation, the degree of absorption can be increased by raising the optical density. The modulation depth, which is about 90% as shown, can be made to be essentially 100% with higher optical density.

4. Experimental set-up

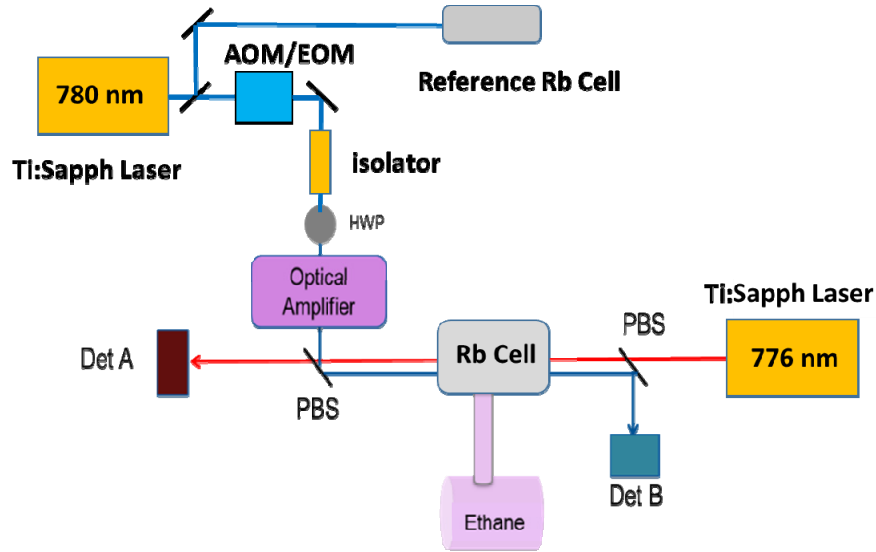


Fig. 4. Experimental set-up for high speed modulator

Figure 4 shows the set-up for the experiment. The 780 nm and the 776 nm beams were obtained from two different continuous-wave tunable Ti-Sapphire lasers. They were cross polarized, and combined and separated using polarizing beam splitters. Both beams were focused to a spot size of about $50 \mu\text{m}$ in diameter. We used an acousto-optic modulator (AOM) or an electro-optic modulator (EOM) for modulating the pump beams. In either case, the power at the output of these modulators is very small and is not sufficient to saturate the buffer gas broadened absorption profile. This necessitated the use of an optical amplifier.

However, since our particular amplifier (a tapered amplifier) works only for a certain input polarization, a half wave plate was added before it. Furthermore, an optical isolator was added after the output of the modulator to prevent feedback from the amplifier. The cell was constructed using conflat flanges with a 4-way cross at the center, providing for two windows for the beam paths, and one each for connecting the Rb reservoir and the Ethane gas tank. A valve, placed between the chamber and the Ethane tank, was closed during the use of the cell as a modulator. Connections were also provided for a mechanical pump, which achieved a pressure of 10^{-3} Torr in the absence of any buffer gas. The Rb cell was heated to approximately 150° C. A buffer gas pressure of typically ~ 300 Torr (~ 6 psi) was used during the experiment. A separate, sealed Rb vapor cell was used to lock the frequency of the pump laser to the D2 transition.

5. Results

The spectroscopic details and the absorption line shapes for the 5S-5P-5D transitions can be found in several publications [12,29–32]. In the absence of the Ethane buffer gas, and for a counter-propagating geometry (as employed in our experiment), the linewidth of the 2-3 transition is expected to be essentially Doppler-free [33]. Of course, the actual spectrum observed depends on the exact frequency of the pump applied on the 1-2 transition, as well as the power of this pump [6,7]. In the presence of the high-pressure Ethane buffer gas, however, all the individual hyperfine transitions are washed out, resulting in a single, broad absorption peak. For example, for an Ethane gas pressure of ~ 250 Torr (~ 5 psi), and pump and probe powers of ~ 760 mW and ~ 0.5 mW respectively, the observed linewidth of the 776 nm probe absorption was found to be ~ 2 GHz, as shown in Fig. 5. The value of $\Gamma_D (= \gamma_d)$ for this pressure is ~ 5 GHz. If the width of this spectrum were to be attributed solely to the collisional dephasing rate ($\beta\gamma_d$), it would imply that the value of β is ~ 0.4 . However, as we discussed earlier, the width of the absorption profile of the 2-3 transition under this condition cannot be ascribed necessarily to this dephasing rate ($\beta\gamma_d$); rather, it is expected to depend on the degree and nature of excitation produced in state 2, which in turn depends on the spectrum, frequency and power of the pump applied on the 1-2 transition. As mentioned earlier, a detailed and systematic experimental study of the absorption processes in this system in the presence of high-pressure buffer gas, augmented by a theoretical model, is necessary to determine the precise value of β (as well as α and ξ). Such a study is underway, and will be reported on in the future. Nonetheless, the significant broadening observed is consistent with our assumption, in the theoretical simulation, that the values of these parameters (α , β , and ξ) are of the order of unity.

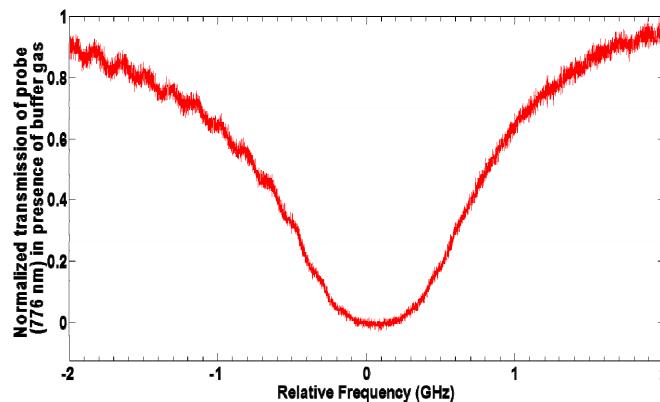


Fig. 5. Probe (776 nm) absorption lineshape in the presence of buffer Ethane. Here, Ethane pressure is ~ 6 psi and the pump and probe powers are ~ 800 mW and ~ 0.5 mW.

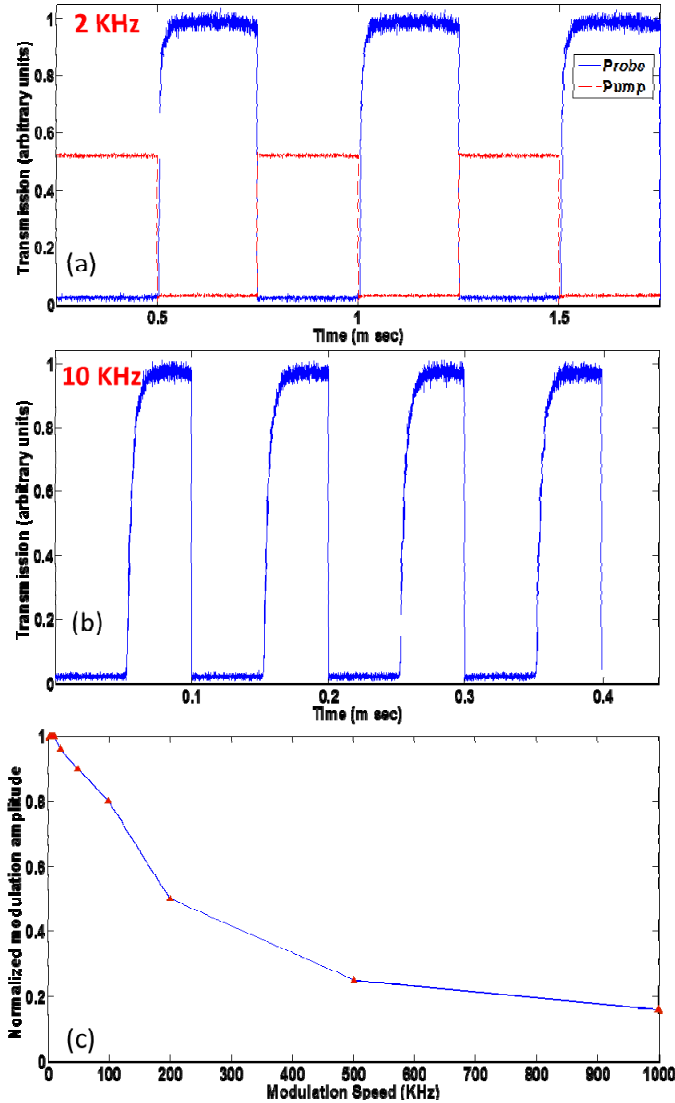


Fig. 6. 5S-5P-5D modulation data without buffer gas. (a) 2 KHz (b) 10 KHz (c) Modulation amplitude vs modulation speed. We have indicated the vertical axes in (a) and (b) as having arbitrary units, since the relevant parameter is the modulation depth, which is about 95% in both cases. In (a), the peak pump signal corresponds to an un-attenuated pump power of ~ 760 mW, and the peak probe transmission corresponds to an un-attenuated probe power of 0.5 mW. Similarly, in (b), the peak probe transmission corresponds to an un-attenuated probe power of 0.5 mW. Since this is an absorptive modulation, the degree of absorption can in principle be increased by increasing the optical density.

Figure 6 shows the results of modulation without buffer gas. The system shows almost perfect square modulation at 2 KHz, as shown in Fig. 6(a). Here, the red trace represents a scaled version of the pump signal. It is not shown in other figures. As is evident from Fig. 6(b), the signal starts to roll off at a frequency of 10 KHz. Indeed, as can be from Fig. 6(c), where we have plotted the modulation amplitude vs. the speed, the bandwidth is about 200 KHz. However, it should be noted that the data shown here is for square modulation. Since a square pulse consists of many harmonics, it is conceivable that the actual bandwidth (for sinusoidal modulation) is 8-10 times larger, i.e. about 2MHz, consistent with the earlier

observation for the 5S-5P-6S system [6]. The power output from the EOMs was too small to produce the desired modulation even with the optical amplifier. Hence, we had to use exclusively the AOMs for our experiments which in turn restricted us to square modulation.

Figure 7 shows the result of the modulation in the presence of buffer gas. With the rest of the conditions remaining identical, we obtained a 100- fold increase in the bandwidth. The rapid decay from state $|2\rangle$ to state $|4\rangle$ caused by the buffer gas results in the probe becoming transparent on a very short time scale, as is evident from Fig. 7. Once again, the data shown is for square modulation and the actual bandwidth is about 200 MHz.

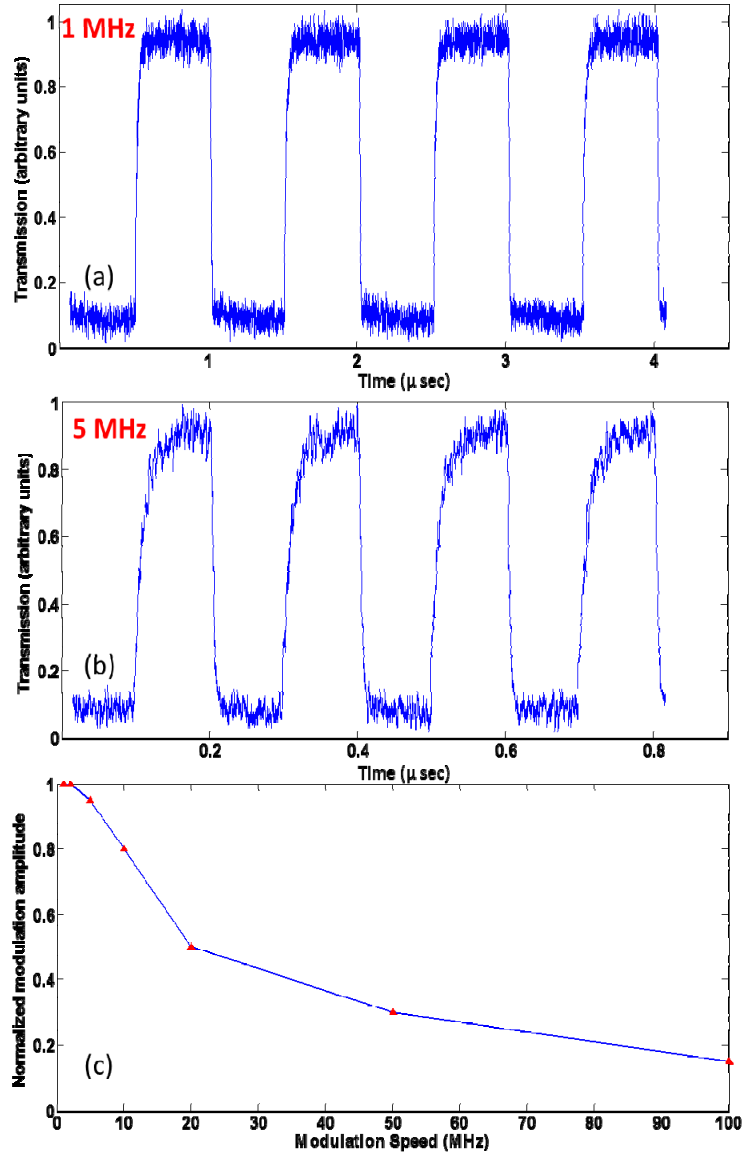


Fig. 7. Modulation data in the presence of buffer gas (Ethane) at pressure of ~6 psi. (a) 1 MHz (b) 5 MHz (c) Modulation amplitude vs modulation speed. We have indicated the vertical axes in (a) and (b) as having arbitrary units, since the relevant parameter is the modulation depth, which is about 90% in both cases. The peak probe transmission at both 1 MHz and 5 MHz corresponds to an un-attenuated probe power of 0.5 mW.

6. Improvements to system and future outlook

As noted above, we observed a 100-fold increase in the bandwidth after the addition of buffer gas, reaching a bandwidth of ~ 0.2 GHz. This is consistent with our model that shows that the bandwidth is bounded by the rate of collisional decay from $|2\rangle$ to $|4\rangle$, which, for the parameters employed here, is $\gamma_{\text{down}} = 0.51$ GHz. Given that it is an absorptive modulator, the bandwidth of the modulation could be increased further (but within the bound set by γ_{down}) by increasing the optical density. One way to do so is to increase the temperature. However, for Ethane buffer gas, a temperature much higher than 150 degrees tends to cause degradation of the windows. The other way to do so is to increase the effective interaction length. For a free space system, this cannot be done without reducing the pump intensity, since the effective interaction length is the Rayleigh length, which depends on the spot size.

On the other hand, it should be possible to increase the bandwidth (up to the limit set by the value of γ_{down}) by using higher pump power. However, our current set up did not allow us to increase the pump power beyond the 760 mW used. Instead, we studied the dependence of the modulation amplitude on the pump power, as shown in Fig. 8. As can be seen, the modulation amplitude keeps increasing monotonically with increasing pumps power, at two different modulation frequencies. From this data, it can be inferred that higher bandwidth would have been observed if we were able to increase the pump power well beyond 760 mW. We did not try to increase the intensity (which, rather than the power, is the relevant parameter) by focusing the beam to a smaller spot, since this process would reduce the Rayleigh length to be much smaller than the current value of ~ 1 cm (for a focused spot size of $50 \mu\text{m}$), which in turn would reduce the modulation amplitude, thus potentially offsetting any enhancement due to increased intensity.

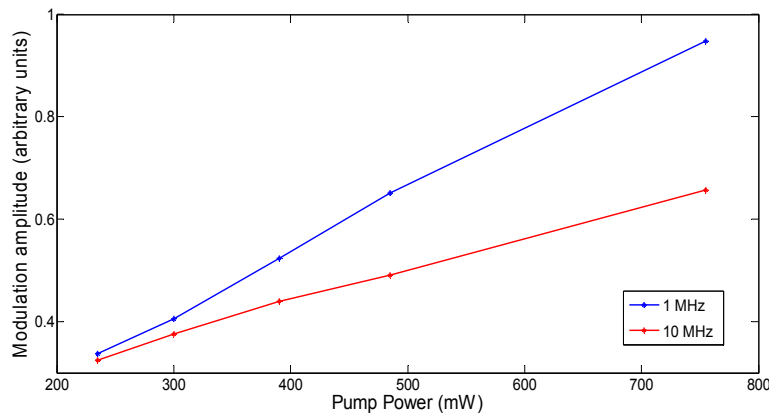


Fig. 8. Increase in modulation amplitude for two different modulation frequencies (1 MHz and 10 MHz) with increase in pump power. Just as in Fig. 6 and 7, the vertical axis is shown in arbitrary units, since the relevant parameter is the modulation depth, which can be increased to be near 100% by increasing the optical depth, since it is an absorptive modulator. The data shown in Fig. 7 correspond to the maximum power employed for the pump beams (760 mW), thus corresponding to the right-most data points in this figure.

Of course, the upper limit of the modulation bandwidth itself can be increased further by increasing the pressure of the buffer gas, thereby increasing the value of γ_{down} , which is expected to vary linearly with the buffer gas pressure up to a value of at least as high as 25 atmosphere [14,27]. Using the fact that this decay rate varies as $1.07 \cdot 10^7 \text{ sec}^{-1}/\text{Torr}$ [14] for Ethane, for a pressure of 25 atmosphere ($= 19000 \text{ Torr}$) the modulation bandwidth would be about 32 GHz. However, given the constraint of our current system on the maximum intensity achievable without reducing the Rayleigh length to be significantly smaller, increasing the pressure beyond the 600 Torr we used would not allow us to observe a higher bandwidth. In

the near future, we plan to use a different experimental system in order to demonstrate higher bandwidth. Specifically, we will use a Silicon Nitride waveguide, embedded in a cell containing Rb vapor as well as high pressure Ethan buffer gas. The core technology for such a system has already been demonstrated [34]. This system has the property that, just like in the case of the TNF, the evanescent field that interacts with the atoms can produce a very high intensity at a very low power. Furthermore, unlike in the case of the TNF, the interaction length can be made very long. One of the drawbacks of the system is that, in its current incarnation [34], the power throughput is very small due to inefficient input coupling. This problem can be circumvented by using a tapered section at the input, or using a photonic crystal based coupler.

It should be possible to realize this modulator at a telecommunication wavelength at very low control powers using the tapered nano fiber (TNF) set-up [10], employing the $5S_{1/2}$ - $5P_{3/2}$ - $6S_{1/2}$ system, for which the probe transition is at ~ 1367 nm. The TNF needs to be designed to operate as a single mode fiber for both wavelengths: 780 nm and 1367 nm. We have carried out designs of such a TNF, and have shown that there is a range of taper diameters for which it is possible to have a significant overlap between the evanescent modes at these two wavelengths. The TNF would be embedded in a Rb vapor cell, and pressurized with Ethane buffer gas. The pump and the probe will be combined using a dichroic mirror and launched into the TNF. As a figure of merit (FOM) for implementation in our TNF system, one can use the number of photons in the pump field that are needed to switch the state of the probe from 'off' to 'on'. In order to achieve an intensity equivalent to a free space pump power of 1W for a spot size of $50\mu\text{m}$, the TNF system with a mode area of $0.2\mu\text{m}^2$ would require a pump power of $\sim 80\mu\text{W}$. Assuming a rise time of 2.5 nS for operation at a modulation speed of 200 MHz, the number of pump photons at 780 nm needed for switching would be $\sim 5 \times 10^5$. Of course, a telecom wavelength modulator of this type can also be realized using the SiN waveguide approach discussed above. Allowing for a near unity throughput using one of the configurations (e.g. tapered waveguide section or a photonic crystal at the input) mentioned above, a bandwidth of 32 GHz for the same power level would correspond to an FOM of $\sim 3 \times 10^3$. Of course, to achieve high modulation depth while using the same power, the interaction length (and hence the optical density) has to be much longer than that of the TNF (which is only about 1 cm). As mentioned above, this is easy to achieve for the waveguide, even within the constraint of a small chip, by using smoothly folded patterns [34]. As a comparison with other techniques for low power all-optical modulation [21–24], we find that the instability induced switch has an FOM of 4×10^4 photons [19] while micro-ring resonators based switches have an FOM of 4×10^7 photons [20]. Thus, this approach is a potentially attractive option for low power all-optical modulation.

7. Conclusions

To conclude, we demonstrated a novel high speed all-optical modulator using the $5S$ - $5P$ - $5D$ transition. We homogeneously broadened the transitions by making use of collisional broadening and fine structure mixing induced by high-pressure buffer gas of Ethane. We obtained a bandwidth of ~ 200 MHz, which represents a 100-fold increase in the bandwidth, in comparison to a system without buffer gas. The observed bandwidth is within a factor of 2.5 of what one might expect based on the parameters used in the model of the system we have employed, and is limited by various practical constraints in our experiment. We also present numerical simulations for the system and predict that a modulation speed of as much as 32 GHz should be achievable under suitable conditions, using a SiN waveguide embedded in a buffer-gas loaded Rb vapor cell, using only about $80\mu\text{W}$ of power.

Acknowledgments

This work was supported in part by AFOSR Grant # FA9550-10-01-0228, and the DARPA ZOE program under Grant # W31P4Q-09-1-0014.